Cellulose
https://doi.org/10.1007/s10570-022-04626-2

ORIGINAL RESEARCH

Dewatering of cellulose nanofibrils using ultrasound

Udita Ringania · Joseph Harrison · Robert J. Moon · M. Saad Bhamla

Received: 12 February 2022 / Accepted: 27 April 2022

Abstract Although cellulose nanomaterials have promising properties and performance in a wide application space, one hinderance to their wide scale industrial application has been associated with their economics of dewatering and drying and the ability to redisperse them back into suspension without introducing agglomerates or lose of yield. The present work investigates the dewatering of aqueous suspensions of cellulose nanofibrils (CNFs) using ultrasound as a potentially low-cost, non-thermal, and scalable alternative to traditional heat-based drying methods such as spray drying. Specifically, we use vibrating mesh transducers to develop a direct-contact mode ultrasonic dewatering platform to remove water from CNF suspensions in a continuous manner. We demonstrate that the degree of dewatering is modulated by the number of transducers, their spatial configuration, and the flow rate of the CNF suspension. Water removal of up to 72 wt.% is achieved, corresponding to a final CNF concentration of 11 wt.% in 30 min using a two-transducer configuration. To evaluate the redispersibility of the dewatered CNF material, we use a microscopic analysis to quantify the morphology of the redispersed CNF suspension. By developing a custom software pipeline to automate image analysis, we compare the histograms of the dimensions of the redispersed dewatered fibrils with the original CNF samples and observe no significant difference, suggesting that no agglomeration is induced due to ultrasonic dewatering. We also perform SEM analysis to evaluate the nanoscale morphology of these fibrils showing a width range of 20 nm–4 um. We estimate that this ultrasound dewatering technique is also energy-efficient, consuming up to 36% less energy than the enthalpy of evaporation per kilogram of water. Together with the inexpensive cost of transducers (< $1), the potential for scaling up in parallel flow configurations, and excellent redispersion of the dewatered CNFs, our work offers a proof-of-concept of a sustainable CNF dewatering system, that addresses the shortcomings of existing techniques.

Keywords Dewatering · Ultrasonic dewatering · Cellulose nanofibrils · Energy-efficient · Continuous platform

Supplementary Information The online version contains supplementary material available at https://doi.org/10.1007/s10570-022-04626-2.

U. Ringania · J. Harrison · M. S. Bhamla (✉)
Chemical and Biomolecular Engineering, Georgia Tech, Atlanta, GA 30332, USA
e-mail: saadb@chbe.gatech.edu

R. J. Moon
The Forest Products Laboratory, U.S. Forest Service, Madison, WI 53726, USA

Introduction

Cellulose nanofibrils (CNFs) are nanosized cellulose particles (20–100 nm in diameter, microns in length)

Published online: 24 May 2022

that have a unique combination of characteristics: renewable, sustainable, biodegradable, low toxicity, high aspect ratio, high surface area, high mechanical properties, transparency, self-assembly, industrial scale production, etc., which gives them utility across a wide range of applications in composite materials, coatings, membranes, biomedical, rheology modifiers, etc. (Moon et al. 2011; Rebouillat and Pla 2013; Geng et al. 2018; Patel et al. 2019; Čolić et al. 2020; Nigmatullin et al. 2020). Although CNFs present many promising properties, one hinderance to their wide scale industrial application is associated with the economics of their processing and handling. Due to their hydrophilic nature, CNFs are processed in aqueous form with the final suspension of about 90–97 wt.% of water (Rebouillat and Pla 2013), leading to high shipping costs. This cost can be circumvented by shipping a dewatered (i.e.., concentrated) or dried form of these materials. However, drying is a cost intensive process (Miller et al. 2015), and can cause permanent changes to CNF nano-dimensional particle morphology, and thus performance. As the water is removed from the system, hydroxyl groups of neighbouring particles get closer resulting in strong hydrogen bonds and triggering agglomeration. Redispersion of these dried particles into stable suspensions that are comparable to that of the original particle dimensions is an ongoing challenge due to the high energy requirements to break these hydrogen bonds (Beck et al. 2012; Missoum et al. 2012; Beuguel et al. 2018). Traditional drying methods such as oven drying, spray drying, freeze drying, suffer from loss of nanoscale dimension due to agglomeration of fibrils associated with inter-particle hydrogen bonding (Peng et al. 2012a). Supercritical drying (Zimmermann et al. 2016) and solvent replacement drying (Hanif et al. 2018) are two methods that has been observed to retain the nanoscale dimensions. However, high cost of operations and complexities associated with scaling up has limited their wide scale application. The advantages and disadvantages of different drying methods used for cellulose nanomaterials (CNMs) is summarized in Table 1.

Apart from drying, which aims at removing all the water from the suspension, a partial drying approach that concentrates a suspension, referred to as `dewatering', has also been employed for CNMs. One advantage of dewatering is that it can avoid CNM agglomeration challenges. Examples of a few common dewatering techniques (Sinquefield et al. 2020), summarized in Table 2, include centrifugation, filtration, shear-induced dewatering and pressing, with variable success in CNMs. Centrifugation and filtration are widely used laboratory scale processes; however, scale-up issues inhibit their integration in industries. A main disadvantage of filtration is the long time required for dewatering (1–4 h/100 ml suspension) (Iwamoto et al. 2005; Sehaqui et al. 2010). Electro-assisted filtration for microfibrillated cellulose (MFC) helps tackle this issue (10–30 min/100 ml of diluted suspension) but only through an increase in the overall energy consumption (Wetterling et al. 2017). Electroosmotic filtration for CNCs has been demonstrated to be energy efficient as compared to the thermal methods, however, higher dewatering rates increases these energy requirements and their applicability to CNFs remains unknown (Wetterling et al. 2018). Other methods using filtration have employed additives such as salts (Sim et al. 2015) and wood pieces (Amini et al. 2019) to assist in phase separation for CNFs, however their recovery is either not feasible or economically unviable. Application of ultralow shear stress to CNFs and MFCs slurry is another approach through which phase separation and dewatering has been achieved (Dimic-Misic et al. 2013, 2017, 2018). However, the approach requires long durational stress application and also results in auto flocculation of the fibers. Finally, subjecting MFCs to high pressure pressing also helps dewater the slurry (Rantanen and Maloney 2015). This is at times assisted with heat (Clayton et al. 2006), or using a plate and frame type pressing mechanism. Thus, with the availability of the present dewatering techniques (Table 2), a low cost, scalable, energy-efficient method is still lacking for dewatering CNMs.

The hypothesis of this study is that ultrasonic approaches can be applied to the dewatering of CNF suspensions. To the authors knowledge ultrasound approaches have not been reported for the dewatering of CNF suspensions, however, ultrasound has been used as a low heat drying method for food, fabric and variety of other solid materials with defined structure (Boucher 1959a; García-Pérez et al. 2015; Musielak et al. 2016; Peng et al. 2017a; Sabarez et al. 2019). The first acoustic drying, as performed by Boucher (1959b, a) and Greguss (1963), used mechanically generated sound in the sonic and ultrasonic range to dry cotton fiber and a wide variety of other materials.

Table 1 Drying methods used for CNMs

Drying method	Advantages	Disadvantages	References
Air drying	Low cost Low energy requirements	High agglomeration Poor redispersibility (irreversible) Loss of nanoscale dimensions	(Peng et al. 2012b; Penttila et al. 2012)
Oven drying	Economical and scalable Established industrial technology	High agglomeration Poor redispersibility Loss of nanoscale dimensions	(Quiévy et al. 2010; Peng et al. 2012a; Zimmermann et al. 2016)
Freeze drying/ Lyophilization	Nanoscale dimensions maintained in parts of the fiber Relatively stable process Well established and scalable process	Agglomeration to a certain extent can occur Slow process High energy requirement	(Peng et al. 2012b, 2013; Han et al. 2013; Zimmermann et al. 2016)
Spray drying	Scalable and fast process Re-dispersible to a certain extent (in micro-nanosized particle range) Continuous process	High installation and maintenance cost Energy intensive Some extent of agglomeration Loss of nanoscale dimension (particle size ranges from nano to micrometers)	(Quiévy et al. 2010; Peng et al. 2012b; Park et al. 2017; Al Zaitone 2019)
Supercritical extraction*	Efficient drying Maintains the nanoscale	Expensive method Complex process Hard to scale up Not applicable to cellulose nanocrystals (CNCs)	(Peng et al. 2012a, 2013; Peng and Gardner 2013; Zimmermann et al. 2016)
Solvent replacement drying (t-BuOH)	Accelerated drying rates (~3 time for oven drying and ~ 3–20 times for freeze drying) than drying rates for original solution Reduced shrinkage during drying process Easy redispersion Maintains the nanoscale structure	100% solvent replacement not achieved Presence of t-BuOH on the cellulose particles after drying	(Hanif et al. 2018)

*Applicable to CNFs only

The extremely small 1–2 °C increase in temperature during the drying process suggests applicability to drying of heat-sensitive materials and high value-target. However, poor energy efficiency and high sound levels due to the air-jet sirens used decades ago hindered the potential applications of mechanically generated acoustic drying. Nevertheless, increasing availability of modern piezoelectric transducers in the recent decades, producing ultrasound energy at significantly lower power inputs, lower audible sounds and with high energy efficiency, rekindled an interest in ultrasonic acoustic drying. Since then, ultrasonic drying has been successfully demonstrated for a variety of food products with a significant reduction in both drying time and energy used (Gallego-Juárez et al. 2007; García-Pérez et al. 2015; Musielak et al. 2016). Recently, ultrasound has also been implemented in fabric drying showing approximately 10 times reduction in energy use as compared to traditional heat based dryer (Peng et al. 2017a, b).

The mode of application of the ultrasound to the sample plays an important role on the final drying efficiency achieved. The two primary modes of application are (i) non-contact mode (or air-borne ultrasound) where the ultrasound is applied to the sample through a medium, usually air, and (ii) direct-contact mode where the ultrasound is directly applied to the sample. Air-borne ultrasound has been observed to assist the convectional air drying but suffers from significant energy attenuation due to mismatch in

Table 2 Dewatering methods for CNMs

Dewatering method	Advantages	Disadvantages	Ref
Centrifugation	Easy availability	Difficult to scale up High energy requirement Batch process	(Astorsdotter 2017; Amini et al. 2019; Zhai et al. 2020)
Filtration* Electro-assisted filtration** Electro-osmotic filtration***	Easy availability* Faster dewatering times**	Long dewatering time*,*** Difficulty to scale up Higher energy requirements Batch process	(Iwamoto et al. 2005; Sehaqui et al. 2010; Wetterling et al. 2017, 2018; Sethi et al. 2018)
Shear induced dewatering	High dewatering efficiency	Induces agglomeration Long dewatering times Batch process	(Dimic-Misic et al. 2013, 2017, 2018)
Pressing	High dewatering efficiency Can be redispersed	High pressure requirements Applicable mainly for longer fiber dimensions (microfibrillated cellulose) Batch process	(Clayton et al. 2006; Rantanen and Maloney 2015)
Ultrasonic dewatering	Continuous process Energy-efficient Easily Scalable Fast dewatering times	Needs modification for application to CNCs	This study

*, ** and *** represent the methods Filtration, Electro-assisted filtration and Electro-osmotic filtration respectively as also seen in column 'Dewatering method'

impedance between air and solid/liquid media. In contrast, direct-contact mode ultrasound ensures a better transfer of energy from the piezoelectric transducer to the solid/liquid in contact (Gallego-Juárez et al. 1999). For highly shrinkable food products during ultrasonic drying, applying a static pressure to the sample ensured constant contact during the entire process effectively reducing the drying time by 65–70% as compared to heated air drying (Gallego-Juárez et al. 2007). More recently, direct-contact mode has been used for dewatering knitted fabrics (Peng et al. 2017a). The low cost and easy availability of piezoelectric transducers used to produce ultrasound motivates this current work to explore the possibility for designing a low-cost direct-contact mode dewatering platform for CNFs.

In this study, ultrasound as a potential low-cost dewatering technique for CNF suspensions is investigated. A direct contact mode approach is undertaken and the effect of system parameters such as suspension flow rate and transducer configuration on the dewatering rate and amount of water removed is studied. The viability of the ultrasonic dewatered material to be redispersed back in suspension is tested along with potential changes in CNF particle morphology. A quick effective and quantitative image analysis approach is developed for visualizing the fibrils in the solution phase using phase contrast microscopy combined with image analysis via a MATLAB code. Histograms generated thereby are compared with original fibrils to identify any changes in morphology or fibril dimensions as a result of dewatering.

Materials and methods

Cellulose nanofibers

Cellulose nanofibers (CNFs) at a concentration of 3 wt.% solids in water (Lot# U-103, 90% fines retained) are procured from University of Maine, Orono, ME, USA (UMaine) (UMaine The Process development Center 2021). These CNFs are generated through mechanical fibrillation of wood pulp and are often branched or forked with dimensions about 20–500 nm in width and several microns in length. Measurements of the solid content for the CNF suspension by us confirmed a concentration of 3.1 ± 0.4wt.% solids.

Vibrating mesh ultrasonic transducer

Ultrasound is produced using a piezoelectric vibrating mesh transducer (VMT) (WHDTS, 20 mm diameter, rated power 1.5–2.5 W, rated voltage 70 V(max) and resonance frequency of 113 ± 3 kHz) which comprises of a metal mesh attached to a piezoelectric ring at the bottom as shown in Fig. 1. The vertical vibration of the metal mesh on application of voltage across the piezoelectric ring generates an acoustic pressure difference that pushes water through the tapered pores of the metal mesh generating a cold mist ejected from the back surface of the transducer (as seen in Fig. 1d and g).

Ultrasonic dewatering

When a CNF suspension is placed on the VMT top surface, the water from the suspension is removed as cold mist while the fibrils does not pass through the metal mesh thereby resulting in the dewatering of the suspension. This system is different from systems such as an ultrasonic spray dryer where the ultrasound is used to atomize the entire CNF suspension thereby forming microdroplets of the CNF suspension. These are then passed through a drying chamber where further thermal evaporation of the solution is carried out to achieve dried CNFs. However, water removal in the present ultrasonic dewatering method is mechanical in approach and does not employ thermal energy.

A direct-contact mode ultrasonic dewatering setup (Fig. 2) is designed such that CNF suspensions can flow over multiple transducers allowing for continuous dewatering. The setup comprises of a syringe pump (kd Scientific 78–0100) to control the flow rate, a 10 ml syringe (inner diameter of the outlet: 1.6 mm), an acrylic transducer stand, VMT, a function generator (RIG01 DG 1022 Function/Arbitrary Waveform Generator) and a power amplifier (Krohn-Hite Model 7602 M) to drive the VMT, a scraper blade pully system operated via external DC motor and finally a collection box to collect the dewatered CNFs. The dewatering that occurs as the CNF suspension flows over the transducers results in a higher viscosity CNF gel-like or paste-like material, thus a scraper blade system is incorporated to assist the gravity driven flow of the CNF material over the transducer plates. The

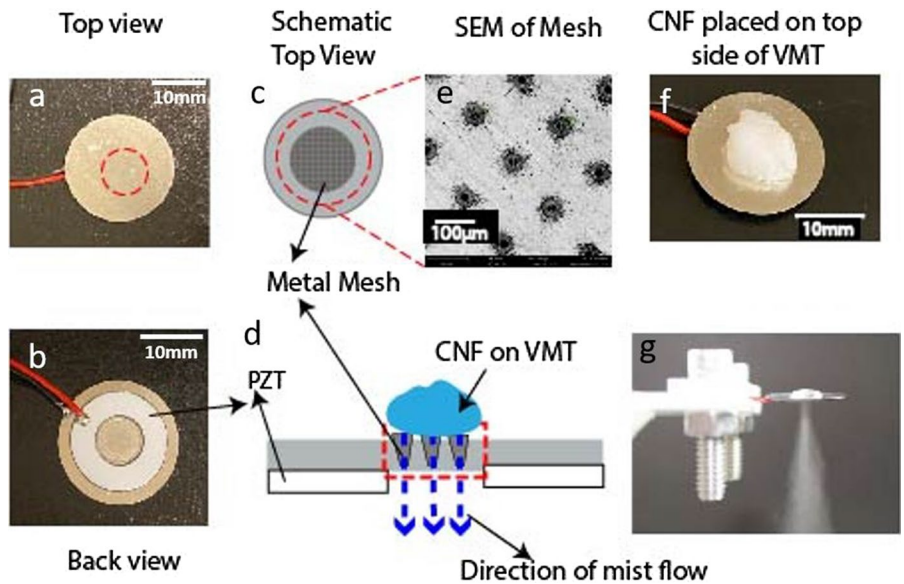

Fig. 1 Vibrating mesh transducer (VMT) comprises of a metal mesh attached to a piezoelectric ceramic ring at the bottom. **a** top view of VMT and **b** back view of VMT. **c** Schematic of the top view of the VMT depicting the metal mesh at the center whereas **d** is the side view schematic of the VMT with CNFs placed on the top surface and water removed from the back surface of the metal mesh. **e** SEM image of the metal mesh with pore size of ~ 18 µm on the top surface. The pores have a tapered geometry with 3–5 µm pore diameter on the back surface. **f** Image of CNF suspension placed on a VMT. **g** Image of a water droplet placed over a VMT actively producing mist from the back surface

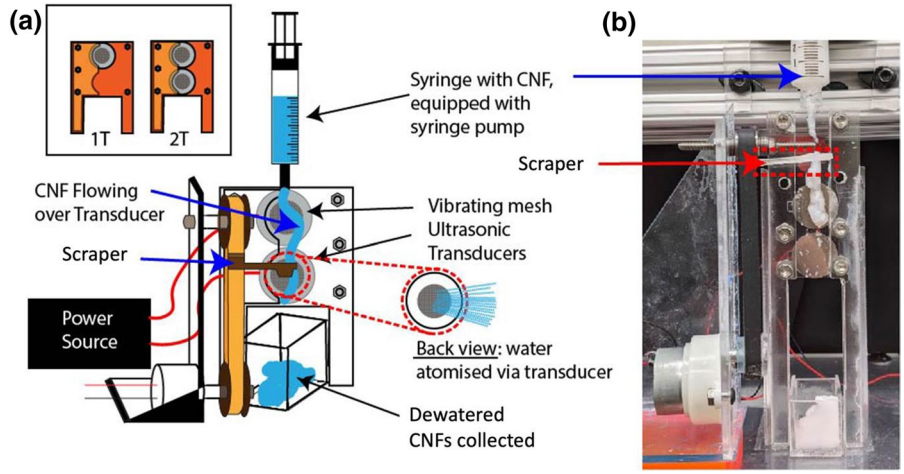

Fig. 2 **a** Schematic corresponding to the experimental setup for the continuous mode ultrasonic dewatering of CNF suspension using VMT. The setup consists of transducer stand, VMT, power source to operate the transducers, scraper with external DC motor to aid the downward flow of the CNF suspension, syringe pump (for controlled dispensing of CNF suspension), 10 ml syringe and a collection box. Inset represents the schematics of the transducer configurations tested. Single transducer configuration (1 T) uses a single VMT for dewatering and double transducer configuration (2 T) uses two VMT stacked vertically one above the other. **b** Image of the experimental setup with the same components. See SI movie 1

velocity of the blade is maintained at 10% higher than the flow rate of the CNFs to achieve a consistent flow over the plate (Online Resource 1: SI-Table 1 and SI-Fig. 1). The flow rate of the CNFs at the syringe outlet and the transducer configuration are varied to assess their effects on the dewatering rate and the amount of water removed. Four flow rates are studied: 60, 30, 15 and 10 ml/hr; and two transducer configurations are used: single transducer configuration (1 T) and double transducer (2 T) configuration (Fig. 2c). At least 4 runs are conducted for each flow rate at each transducer configuration with the initial sample size of 5 ml each (loaded in a 10 ml syringe and initial weight (W_i) recorded using a weighing machine (METTLER TOLEDO ME0204TE/00)). The transducers are operated at 113–117 kHz and 60 Vpeak. The final dewatered samples are collected in the box at the bottom and its final weight is recorded (W_f). Temperature measurements during the continuous flow experiments indicated ~20 °C rise in the suspension temperature over the transducer (see Online Resource 1 SI-Fig. 1). This level of temperature rise is inconsequential for our system as it is below the thermal degradation temperature of CNFs and does not drastically affect the evaporation rates.

Characterization

CNF concentration calculation

The initial concentration of the CNFs in the suspension is ~3 wt.% (C_i). This is used to calculate the initial weight of the CNF solids (F_i in mg) in the sample suspension of initial weight W_i (in mg)

$$F_i = \frac{3}{100} \times W_i \tag{1}$$

The percent of water removed from the system is calculated as follows:

$$\%water\ removed = \frac{W_i - W_f}{W_i} \times 100 \tag{2}$$

Here, W_f is the final weight of the CNF suspension collected after dewatering. The final concentration of the CNFs (C_f) are calculated by assuming that CNF solid content in the suspension remains constant and that no CNFs are lost during dewatering. Hence final CNF solids weight, $F_f = F_i$

$$C_f\ wt.\% = \frac{F_f}{W_f} \times 100 \tag{3}$$

For example, let us start with initial CNF suspension weight of 100 mg with 3 mg of CNF solids. Let us assume that the final weight of the dewatered CNF suspension is 30 mg. Hence, percent water removed = ((100 − 30)/100) *100 = 70%. The final CNF concentration = ((3/30)*100) = 10 wt. %.

Dewatering rate

Dewatering rate, in this study, is defined as the amount of water removed from the system in the time taken for processing 5 ml of CNF suspension at a given flow rate. It is calculated using the following equation:

$$Dewatering\ rate(mg/\min) = \frac{W_i - W_f}{t} \quad (4)$$

Here, t is the time required for processing 5 ml of CNF suspension and is equal to 5, 10, 20 and 30 min for 60, 30, 15 and 10 ml/hr flow rates, respectively.

Redispersion

The dewatered samples are diluted using DI water to 1, 0.1, 0.01 and 0.001 wt.% of CNF solids and redispersed via a vortex mixer (VWR Analog Vortex Mixer No. 10153-838) at speed 7 for 30 s. The original CNF sample with initial 3 wt. % is also diluted using DI water to the above weight percentages and mixed using vortex mixer to form a homogeneous suspension and act as a reference sample.

Microscope imaging

Phase contrast microscopy images of the fibrils for redispersed dewatered samples and diluted original CNF sample each at 0.01 wt.% are taken using an optical microscope (Nikon ECLIPSE Ti2-U). Phase contrast microscopy is a contrast enhancing optical technique that works by converting the phase shifts in light passing through a specimen into changes in brightness in the image. This technique can be directly applied to CNF suspensions thereby providing a fast and easy characterisation tool for analysing fibril distribution and dimensions. The specimens for imaging are prepared by placing a 15 µl droplet of the 0.01 wt% sample in a channel (created by placing double sided tape (thickness: 88.9 µm) ~1.5 cm apart) on a glass slide (VWR VistaVision™ Cat.No. 16004-430 (76.2 × 25.4 × 1) mm) and covering using a glass cover slip (Thermo Scientific™ Gold Seal™ Cover Glass (25 × 25) mm No1). Images are taken using the 20x objective lens and the phase 1 contrast filter. At least 3 sets of microscope samples are prepared for each dewatered sample and at least 5 images at various points of each microscope sample are taken.

Image analysis and microscale redispersion assessment

The phase contrast microscopy images are selected for image analysis on account of their desired contrast, clarity, and fibril density. Original CNF samples (reference sample) and dewatered samples are analysed via modified version of a MATLAB code (GTFiberUND), which is uploaded in GitHub. Changes in fibril lengths and widths induced by ultrasonic dewatering relative to the original sample are assessed. The resulting length and width data are compiled into histograms.

Contrast scanning electron microscope imaging

Contrast Scanning electron microscopy (SEM) images for redispersed dewatered fibrils and diluted original fibrils at 0.001 wt % are taken using benchtop SEM (Phenom Pure). As CNFs are non-conductive material, these images are taken using contrast SEM imaging technique by placing the fibrils on a highly conductive substrate. The benefit of this technique is that coating of the CNF material is not needed and facilitates analysis of the nano-sized fibril structures. As SEM cannot image non-conductive materials, a high contrast image is generated between the conductive imageable substrate and the non-conductive fibril. The specimens for imaging are prepared by placing 3 droplets of 2 µl each of the 0.001 wt. % sample at 3 locations on a silicon wafer, and left to air-dry overnight. At least 3 images are taken for each droplet at three different magnifications and repeated for all the samples.

Image analysis and nanoscale morphology assessment

The SEM images are used to measure the fibril width using ImageJ to assess the nanoscale morphology of the fibrils before and after ultrasonic dewatering. Due to the lack of a better method (automated) for measuring these dense networked fibrils, the measurements are done manually. Every fibril is followed along its length and fibril width is measured for each branching. Measuring the same branch at multiple points is avoided as best as we could. At least 3 images for each sample are measured and the resulting width data are compiled into histograms.

Results and discussion

Mechanisms of ultrasonic dewatering

For this study vibrating mesh transducer (VMT) is used to generate high frequency pressure waves. The main distinguishing feature of these transducers is the presence of a metal mesh at the center (Fig. 1a, c, e) supported by a piezoelectric ceramic ring at the back (Fig. 1b), which vibrates at high frequencies (resonance frequency: 113–117 kHz) on application of voltage. The metal mesh has a tapered geometry with the smaller diameter opening at the back surface (diameter: 18 µm at top surface and 3–5 µm at back surface). When a water droplet is placed on a VMT, the vibration of the metal mesh creates a pressure gradient that pushes the water through the pores resulting in the ejection of water through the back surface as a mist (Fig. 1d and f). The vibrations also result in surface instabilities generated at the air-water interface of the droplet at the front surface of the transducer, resulting in droplet atomization. Thus, the VMT helps eject water as a combination of mist ejection from the mesh and droplet atomization from air-water interface.

To evaluate if water could be separated from a CNF suspension (instead of a pure water droplet), we place a droplet of CNF suspension (~ 200 mg) on the VMT and subject it to ultrasonic vibrations. We observe that the liquid from the system is ejected through the back surface of the metal mesh (Fig. 1d shows a schematic representation of the water ejected through the mesh) while a secondary liquid removal via atomization is observed from the top surface at the CNF suspension-air interface. This secondary atomization is verified using a 'glass slide test' (Online Resource 1 SI-Fig. 3) as the atomization intensity is small compared to that of a pure liquid making it difficult to detect via visual inspection.

The presence of CNFs in the water ejected through the mesh is tested by analyzing the solids content of the ejected water (i.e., the water was collected, allowed to dry, and the solids weighed). It is found that the fibrils ejected through the system in the water is insignificant. However, a very small quantity of CNFs was seen on the back surface of the transducer mesh stuck to the plate at the end of the runs; their measured weight is insignificant (~ 0.001 times the initial CNF weight in the starting suspension). Here we hypothesize that, as water is removed from the system, the fibrils come closer together creating a network that prevents the passage of CNFs through the metal mesh. Thus, the ultrasonic waves act to remove the unbound excess water in the CNF suspension.

Continuous ultrasonic dewatering of CNF suspensions

Having established the feasibility of ultrasonic dewatering of CNF suspensions using VMT, we designed an ultrasonic dewatering platform that can operate as a continuous system (Fig. 2). A continuous platform allows for faster operation times compared to a batch process and potential incorporation into an existing industrial process. The present design allows precise control of the CNF suspension flow rate by using a syringe pump, as well as an easy means of changing the transducer configuration. It must be noted that we control the flow rate of the suspension at the syringe outlet rather than at the transducer surface which can get effected by various parameters such as gravity-effects, scraper blade velocity and changing viscosity of the suspension undergoing dewatering. Dewatering experiments focused on the effect of suspension flow rates and transducer configurations (e.g., 1 and 2 T) on the extent of dewatering of CNF suspensions.

Effect of flow rate

For the single transducer configuration water removal from 3 wt.% CNF suspension is 16.3 ± 0.9, 23.6 ± 4.0, 36.4 ± 3.4 and 55.6 ± 11.7wt.% for

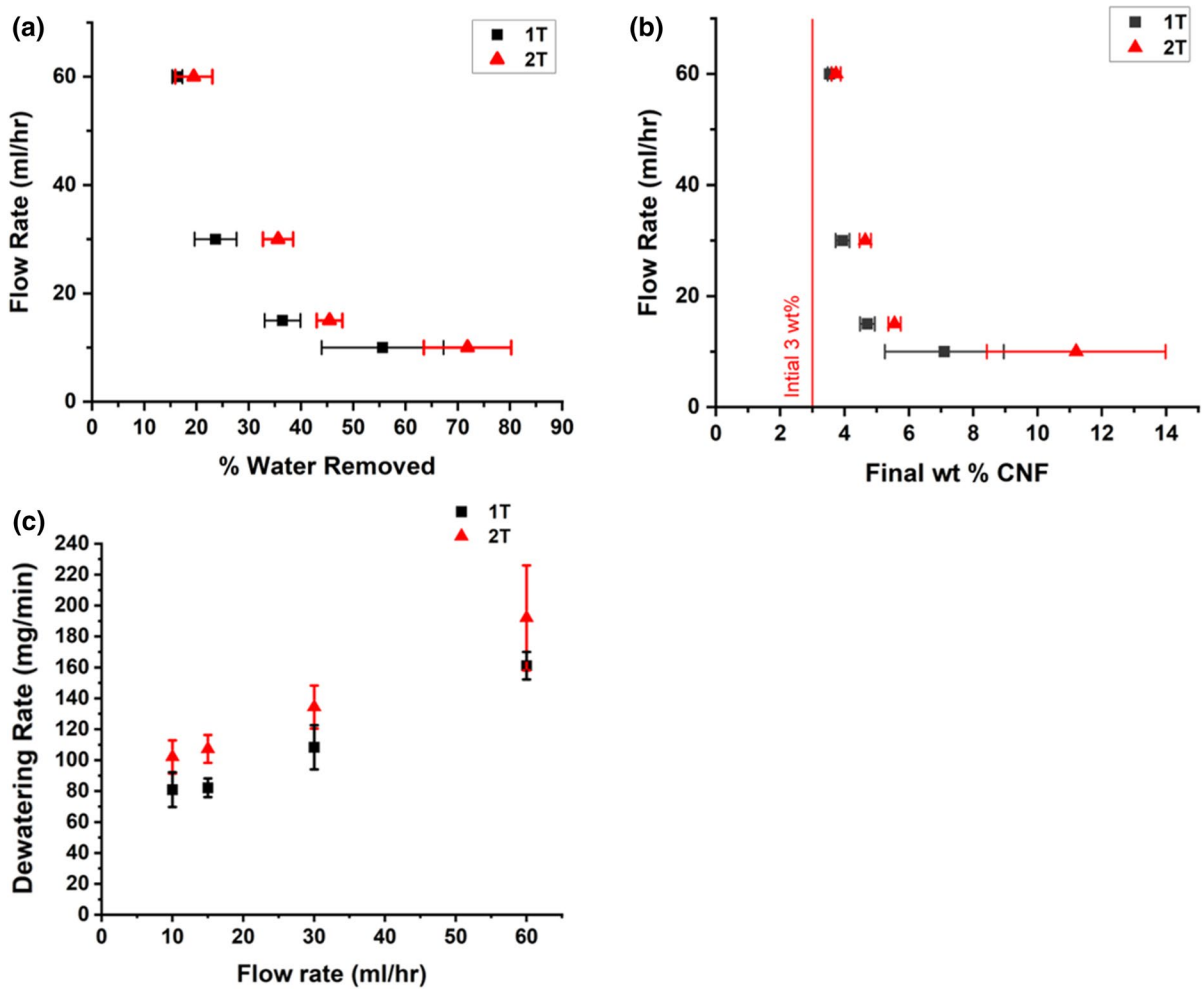

Fig. 3 **a** wt. % of water removed and **b** the final concentration of CNFs in wt.%, at various flow rates during the continuous flow ultrasonic drying using VMT. The data were collected for two transducer configurations: single transducer (1T) and double transducer (2T). **c** Dewatering rate of the various flow rates and transducer configuration

60, 30, 15 and 10 ml/hr flow rates, respectively (1 T, Fig. 3). The percentage of water removal demonstrates an inverse relation with the flow rate of the CNF suspension over the transducer, increasing with lower flow rates. The highest final CNF concentration (at 1 T configuration) of 7.1 ± 1.8wt.% is achieved at the lowest flow rate of 10 ml/hr. These results suggest that lower flow rates ensure higher contact time (residence time) between CNF suspension and the transducer surface, thereby ensuring higher exposure to the ultrasonic waves and higher extent of dewatering.

For the 2 T configuration, a similar inverse trend between flow rate and percent water removal is observed, but the level of water removal is higher. Water removal for 60, 30, 15, and 10 ml/hr flow rates are 19.5 ± 3.5, 35.6 ± 2.9, 45.4 ± 2.5, and 71.9 ± 8.3wt.%, respectively. The highest water removal of 71.9 ± 8.3wt.% (Fig. 3a) (for 2 T configuration) occurred at 10 ml/hr flow rate, and resulted in a final CNF concentration of 11.2 ± 2.8wt.% (Fig. 3b).

However, at lower flow rates (10 ml/hr and lower), a low-pressure induced seperation of CNFs from the water is observed within the syringe. This leads to the water being pushed out of the syringe while the CNFs form a compact network in the syringe making it difficult to pass through the syringe nozzle (see Online Resource 1: SI-Fig. 4). An inhomogeneity in the

initial CNF concentration exiting the syringe occurs, resulting in the higher error bars for these experimental sets (at 10 ml/hr, Fig. 3). Such phase separation becomes severe for the 5 ml/hr flow rate experiments and hence, flow rates below 10 ml/hr are not feasible for the present setup.

Effect of transducer configuration

Understanding the effect of transducer configuration on dewatering at any given flow rate can help determine the optimum operational conditions and give insight into scale-up potential of this platform. For any given flow rate, the amount of water removed and dewatering rates are higher for the 2 T configuration as compared to the 1 T configuration (Fig. 3). This is attributed to the higher contact area achieved between the CNF suspension and the transducer for the 2 T configuration. Interestingly the amount of water removed at the fastest flow rate of 60 ml/hr is similar for both the configurations, suggesting that there exists a critical residence time between the suspension and the transducer surface for the effects of the vibrations to significantly manifest in the system. Thus, below this critical residence time, increasing the contact area (through additional transducers) does not significantly affect the extent of dewatering for the system. Transducers can further be arranged in a sandwiched configuration, with the two transducers facing each other and CNF suspension flowing in between them (Online Resource 1: SI-Fig. 5). The increase in the dewatering extent with an increase in the number of transducers suggests the potential for further scale-up of the system as arrays of transducers can be leveraged to increase dewatering amount at faster flow rates.

Dewatering rate

Dewatering rate for each flow rate at 1 T and 2 T configuration are calculated using Eq. 4 and presented in Fig. 3c. Although higher extent of dewatering is achieved at lower flow rates due to prolonged contact time with the transducer surface (as seen in Fig. 3a), dewatering rates follow a reverse trend. The dewatering rate is directly proportional to the flow rate with highest dewatering rates (161.0 ± 8.9mg/min for 1 T and 192.0 ± 33.9mg/min for 2 T) achieved corresponding to 60 ml/hr flow rate. The dewatering rate decreases to 108.0 ± 14.0, 82.0 ± 6.0 and 80.9 ± 11.0mg/min for 1 T configuration and to 134.0 ± 14.0, 107.0 ± 9.0 and 102.0 ± 10.7mg/min for 2 T configuration at flow rates 30, 15 and 10 ml/hr, respectively. This trend can be explained by the non-linear dewatering behaviour seen for VMT at static dewatering experiments (Online Resource 1: SI-Fig. 6). A direct dependence of the dewatering rate on the transducer number is also observed. Higher dewatering rates are observed at 2 T configuration as compared to the 1 T configuration for all flow rates. Thus, dewatering rate can be leveraged as a design parameter, along with the transducer configuration and flow rates, for future scale-up of our system.

Redispersion of dewatered CNFs

Agglomeration of CNFs triggered by the removal of water is a major disadvantage of dried CNFs, as the particles lose their nano-dimensions and high surface to volume ratio. As many CNF applications require a homogenously dispersed suspension of the fibrils at the nanoscale, successful redispersion of the dewatered samples to attain pre-dewatered dimensions become a crucial processing step. Transmission electron microscopy (TEM) and scanning electron microscopy (SEM), although widely used for assessing redispersion quality due to their nanoscale resolution, comes with inherent challenge associated with deconvoluting the effect of the drying needed in TEM and SEM sample preparation, which often lead to agglomeration triggered by droplet evaporation. Despite this they are acceptable techniques to measure the nanoscale features of CNFs (Kelly et al. 2021). In current work we use contrast SEM imaging technique to visualize and assess the fibril morphology at higher resolution to ascertain the presence of nano-dimensions.

To assess the dispersion state and the potential of agglomeration within redispersed CNF suspensions, a suspension-based characterisation technique is needed. One such technique is Dynamic Light Scattering (DLS), which has been used for calculations of hydrodynamic radius of CNMs (Foster et al. 2018). However, the fibril dimensions used in our study exceeded the size range of operation by DLS, thereby rendering this technique unapplicable in this study. Consequently, we use visual inspection and optical

microscopy imaging of the suspension to evaluate the level of CNF agglomeration.

The extent of CNF agglomeration in the suspension state is assessed in two modes: macroscopically via visual inspection and microscopically via phase contrast optical microscopy. By comparing the original never dried CNF suspension (reference sample) to the redispersed dewatered CNF suspensions, it is considered here that any differences would likely be attributed to the dewatering and redispersion processes. Large agglomeration of the fibrils (> 1 mm in size), identified by the presence of opaque clump like structures in the suspension, are assessed by direct visual inspection of the suspension. This provided a fast and easy initial screening for agglomeration in the redispersed system. Finer scale agglomeration of the fibrils is assessed using phase contrast microscopy imaging to inspect fibril distribution and potential agglomeration in microscale range (between 1 and 1000 μm). Unfortunately, assessing the fibril features and agglomeration in the nano-scale (below 1 μm) is not feasible by optical microscopy, hence, our claims are restricted to the microscale range.

Macroscopic redispersion

Images of the redispersed samples for various flow rates along with reference sample (original 3 wt.% CNF sample diluted to desired wt.%) at 1 and 0.1 wt.% for 2 T configuration are given in Fig. 4 (images for 1 T configuration are presented in Online Resource 1: SI- Fig. 7). Set A are samples at 1 wt.% and Set B are samples at 0.1 wt.%. Visual inspection of the redispersed samples looked very similar to the reference CNF suspension suggesting that no drastic changes in the CNFs due to agglomeration occur in the redispersed state. Even the highest dewatered CNF concentration (i.e. Figure 4 Set A and B, 2 T setup at 10 ml/hr flow rate, corresponding to ~ 11 wt. % CNFs as seen in Fig. 3b) resulted into a well redispersed suspension using the vortex mixture.

Microscopic redispersion

The micro-scale dispersion state and the level of CNF agglomeration is assessed by phase contrast optical microscopy. To assess if dewatering altered the level of CNF agglomeration, the redispersed suspensions were compared to the reference CNF suspensions. Images obtained for the redispersed samples using the phase contrast microscope are presented in Fig. 5 (and in Online Resource 1: SI-Figs. 8 and 9). For each sample, the images were taken at multiple different locations to rule out user bias (~15 images per sample). A comparison with the reference sample revealed that the images for different dewatered samples are visually indistinguishable from each other. At 1 and 0.1 wt.% concentration, the fibril density was quite high forming intertwined networks. Although the fibrils looked well dispersed, at these high densities it was difficult to judge if any agglomeration is taking place (see Online Resource 1: SI-Fig. 8). Hence, suspensions with higher dilution

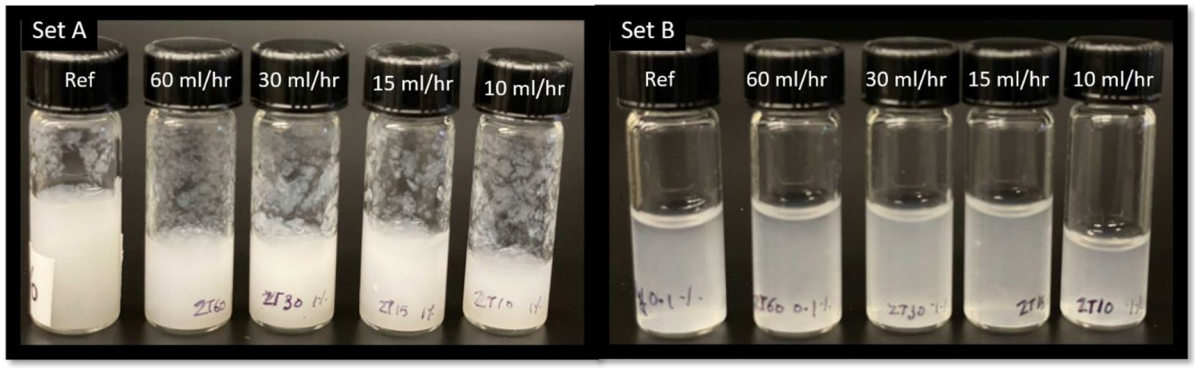

Fig. 4 Redispersed suspensions of ultrasonic dewatered CNFs at various flow rates along with the diluted reference CNF sample for 2 T configuration. Set A: 1 wt.% samples. Set B: 0.1 wt.% samples

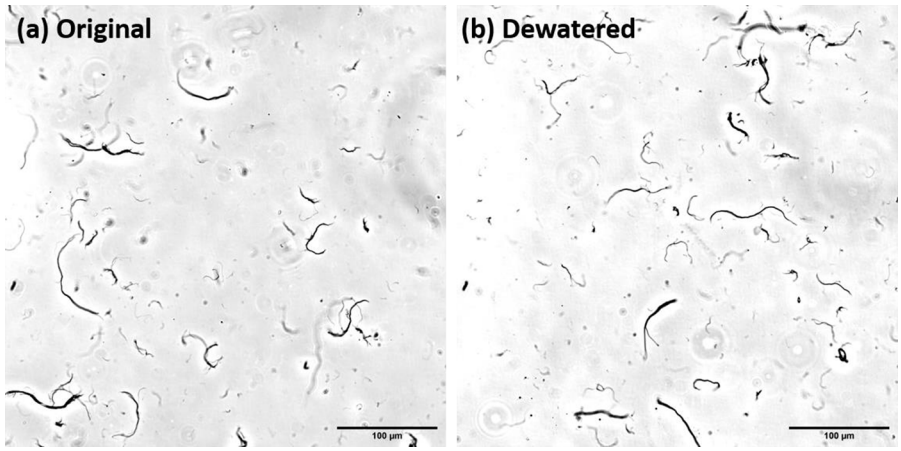

Fig. 5 Phase contrast optical microscopic images using 20× magnification lens for the fibrils in suspension for **a** original CNF sample diluted to 0.01 wt.% and **b** CNF sample dewatered using 2 T configuration at 10 ml/hr., redispersed to 0.01 wt.%

(i.e. 0.01 wt.%) are used to obtain sparsely packed fibril images thereby allowing us to analyse the fibril arrangement and potential agglomeration using the phase contrast mode for imaging.

Optical microscopy images at 0.01 wt.% for a diluted original CNF sample along with a redispersed dewatered sample are shown in Fig. 5a and b respectively (and in Online resource 1: SI-Fig. 9). Long branched fibrils as well as short individual fibrils are seen throughout the suspension in all the samples. The images for the ultrasonic dewatered samples are visually indistinguishable from the original sample. Hence, a more statistical approach is undertaken to assess the potential agglomeration on redispersion of the dewatered samples through analysing the changes in fibril width and length for these samples.

Manual calculation of the length and width of individual fibril is tedious time-consuming work and leads to user bias and manual errors. Hence a computational approach is adapted in this work where all fibrils in each image are analysed using a modified MATLAB code originally designed to analyse fibre dimensions in high contrast imaging techniques such as TEM and SEM (Online Resource 2). The

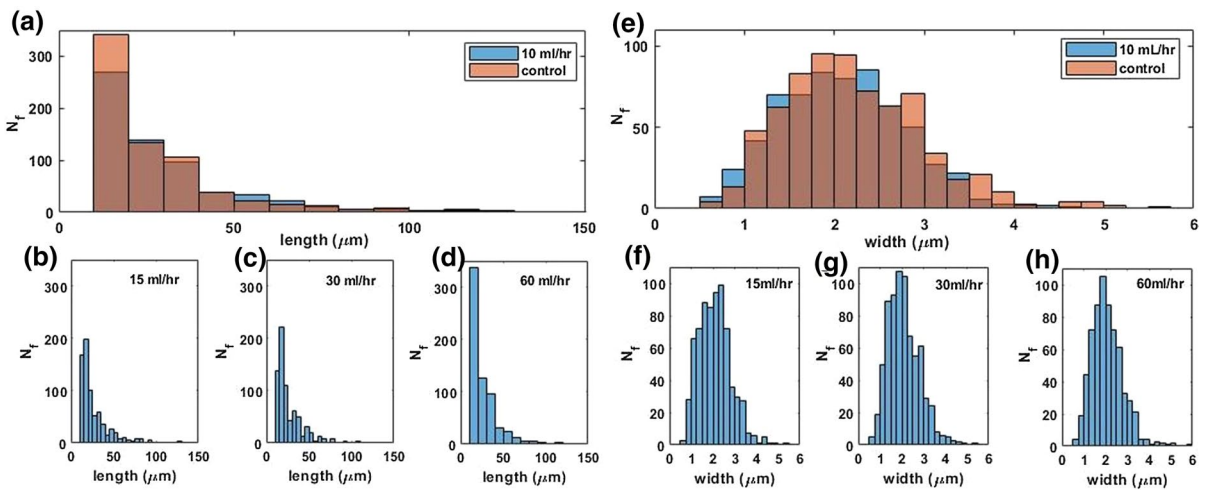

Fig. 6 Histogram data for length and width of the redispersed samples subjected to ultrasonic dewatering at 2 T configuration and various flow rates. At least 10 images (> 600 fibrils) for each sample are analyzed. **a** Fibril length for 10 ml/hr. flow rate samples plotted along with the reference sample. Fibril length data for samples dewatered at **b** 15 ml/hr. **c** 30 ml/hr. and **d** 60 ml/hr. flow rates. **e** Fibril width for 10 ml/hr. flow rate samples plotted along with the reference sample. Fibril width data for samples dewatered at **f** 15 ml/hr. **g** 30 ml/hr. and **h** 60 ml/hr. flow rates

phase contrast optical microscopy imaging technique used in this study successfully generated high contrast images that are compatible to be used with the code. Thus, phase contrast microscopy in combination with the MATLAB code provided a fast and easy fibril characterisation technique for CNF suspensions. At least 10 images (> 600 fibrils) for each sample are analysed. The length and width data for each flow rate and the reference sample are then compiled into histogram graphs as presented in Fig. 6. The length and width histograms have similar distributions for both the redispersed dewatered CNF suspensions and the reference CNF suspension, suggesting minimal microscopic agglomeration effects. The general trend displayed by this analysis for all the flowrates and transducer configurations (Fig. 6 and Online Resource 1: SI-Fig. 10) exhibits that fibril lengths and widths are widely conserved during the ultrasonic dewatering process. This dimensional conservation suggests that the ultrasonic dewatering technique presented in this study successfully removes water from CNF suspensions without inducing much if any permanent agglomeration.

Nanoscale fibril morphology

The nano-scale fibril morphology of CNFs, before and after ultrasonic dewatering, is assessed by contrast SEM imaging. A word of caution here, the drying step necessary for SEM image sample preparation may collapse the fibrils into agglomeration, so the morphology that is measured may not be what is observed in the wet state. Despite this, SEM analysis is used here to confirm nano-size scale features of the CNFs. Contrast SEM images for the diluted original sample at 0.001 wt.% and at various magnification are shown in Fig. 7a and b. These images show the forked, branched nature of CNF samples. The complex nature of the CNFs lends to the difficulty associated with their dimension characterisation and reporting a single width dimension is not a true representation of these morphology. The histogram in Fig. 7e shows that majority of original CNF samples width ranges between 20 and 500 nm. Images for redispersed ultrasonic dewatered samples (dewatered to 11 wt. %) diluted to 0.001 wt.% presented in Fig. 7c and d shows a similar trend in fibril width and is shown in the histogram in Fig. 7f. SEM images along with the width histograms for rest of the samples are present in Online Resource SI-Fig. 11. Thus, these analysis confirm the presence of nanostructure in these fibrils while also confirming that no significant morphological changes occur during the dewatering process.

Benchmarking study

A preliminary benchmarking study is completed to assess the redispersion performance of our ultrasonic dewatered samples with filter-pressed samples (alternate dewatering method) and freeze-dried samples. Filter-pressed CNFs dewatered to 15 wt.% and freeze-dried CNFs, were obtained from the Process Development Centre at UMaine. Microscopy images of the redispersed samples are presented in Online resource SI-Fig-12 (optical images), and SI-Fig-13 (SEM images), and also includes brief description of the findings. In general, the filter-pressed and freeze-dried samples did not redisperse as well as the ultrasonication method used in the current study. The high level of CNF agglomeration complicated image analysis (optical and SEM) of filter-pressed and freeze-dried samples and could not be completed with current approaches used in this study.

Energy consumption to dewater

The existing dewatering and drying methods for CNFs are highly energy intensive, thereby making it important to develop energy-efficient and economically sustainable dewatering/drying methods. Ultrasonic dewatering system for CNFs is developed with these goals in mind and estimation of its energy consumption is conducted. Based on the power rating for a single VMT used in this study i.e. 2.4 J/s, the energy consumed by the ultrasonic dewatering platform is estimated for per kilogram of water removed. For this calculation, we assume that the system is operating at 1 T configuration and 10 ml/hr flow rate of the CNFs, which takes 30 min to dewater 5 g of a 3 wt.% CNF suspension. The dewatering time is extrapolated for removal of 1 kg of water from CNF suspension and the energy consumed by the system is estimated to be ~ 1543 kJ/kg of water removed (summarized in Table 3). A comparison of the 2 T system with the 1 T system is also presented in Table 3.

Energy consumption data for CNM dewatering processes such as centrifugation, filtration, shear

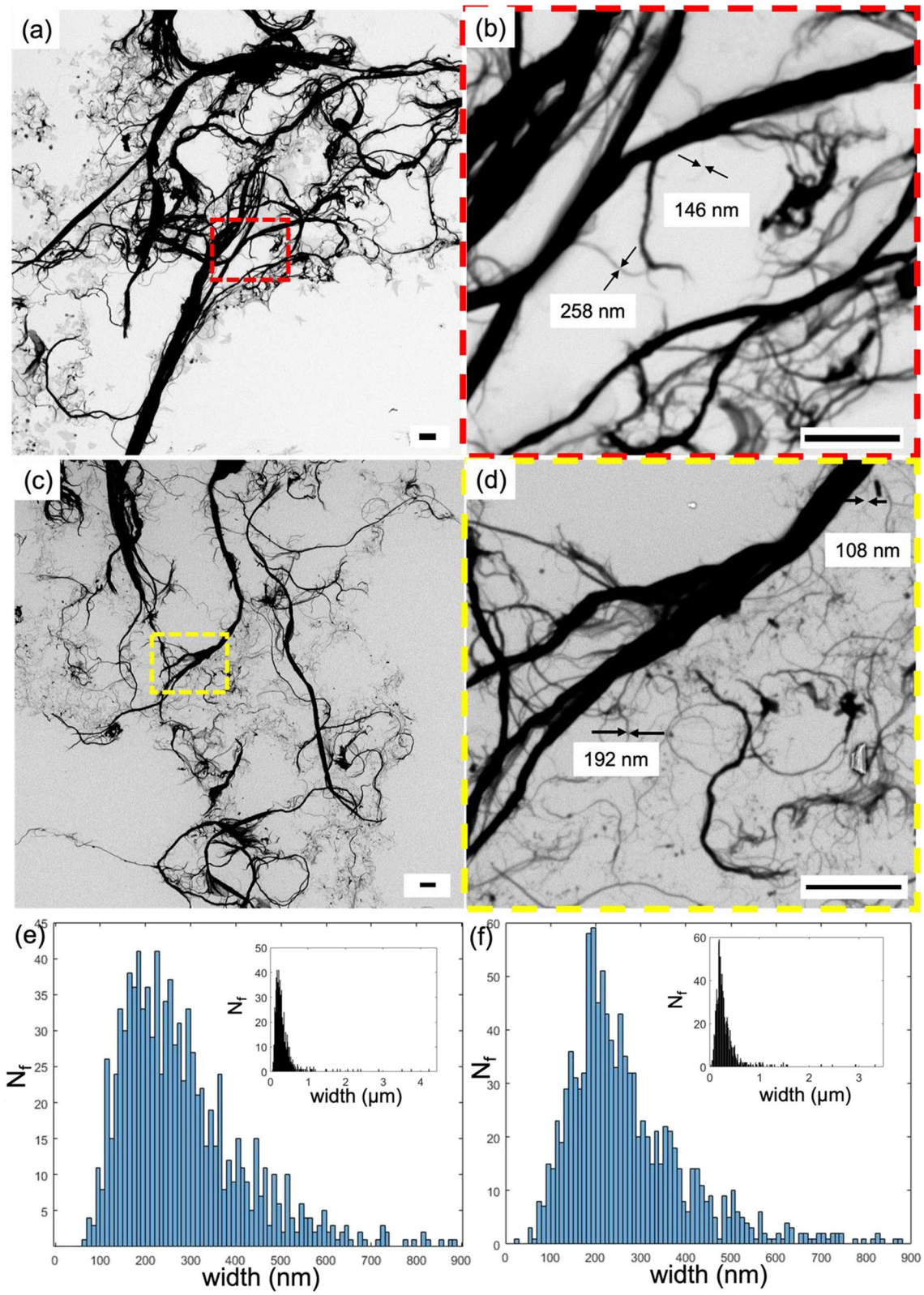
(a)
(b)
146 nm
258 nm
(c)
(d)
108 nm
192 nm
(e)
(f)
N_f
width (nm)
width (μm)

◂**Fig. 7** Contrast SEM images of **a**, **b** original CNF suspension diluted to 0.001 wt.% **c**, **d** CNF suspension dewatered to 11 wt. %, redispersed and diluted to 0.001 wt.%, at different magnification. Scale bars are 10 µm. Histogram of the widths of the **e** original fibrils, **f** ultrasonic dewatered fibril to 11 wt. % and redispersed to 0.001 wt.%, both showing most of the fibril width ranging between 20 and 500 nm. The insets show fibrils width ranging between 20 and 4 µm, a demonstration of the complex nature of these fibrils

induced dewatering or pressing is not available in literature to the best of our knowledge. While energy consumption comparison with these methods would have been ideal, we evaluate our system based on thermal drying systems to offer a rough estimate. The enthalpy of evaporation of water at 25 °C is 2441.7 kJ/kg (Engineering Toolbox 2010), which is the minimum energy that must be supplied for any thermal drying system. The average energy consumption value for an industrial spray drier, the most widely used drying technique for CNMs, is ~ 5469 kJ/kg of water removed (Baker and McKenzie 2005) which is significantly higher than the estimated energy consumption for the ultrasonic dewatering system. It is also worthwhile mentioning that the transducers used in this study are inexpensive (< $1 each) and are easily available for bulk purchase. Thus, the low energy requirements of these transducers along with their low capital cost makes ultrasonic dewatering a promising energy efficient and economically viable alternative for dewatering of CNFs.

Conclusion

A new dewatering technique that uses ultrasonic transducers to remove water from the CNF suspension is introduced in the present work. The custom build ultrasonic dewatering platform is shown to efficiently remove water from the system without triggering agglomeration of the fibrils. The flow rate and the spatial transducer configurations are varied to study their effect on the dewatering performance. Decreasing the flow rate of the CNF suspension resulted in an increase in the amount of water removal for the system. This is due to the increased residence time of the suspension over the transducer surface. However, the trade-off for increased dewatering is longer dewatering durations (due to lower flow rates) along with the higher inconsistency in the amount of water removed (higher error bars) due to the low-pressure induced phase separation within the syringe at lower flow rates. On the other hand, increasing the number of transducers increases the amount of water removed for all flow rate through an increased working contact area between the transducer and the suspension. The dewatering rate for our system is found to be directly dependent on the flow rate as well as the transducer number as a result of the non-linear dewatering behaviour of the transducer. Up to 72% of water removal is achieved, corresponding to a final CNF concentration of ~ 11 wt.%.

The redispersion of the dewatered samples achieved via vortex mixing resulted in homogeneous suspensions with no additional agglomeration observed on visual inspection. Further analysis using

Table 3 Overview of operational and economical parameters for the ultrasonic dewatering platform

System	Initial weight	Dewatered water %	Time taken	Final CNF concentration	Energy consumed
1 T	5 g of 3wt.% CNFs	~56 wt. %	30 min	~7 wt.%	~1543 kJ/kg of water removed
2 T	5 g of 3wt.% CNFs	~72 wt.%	30 min	~11 wt.%	~2400 kJ/kg of water removed

phase contrast microscopy provided a fast and easy technique for microscale visualisation of these fibrils. Dimensional analysis of the fibrils revealed a similar histogram distribution for the redispersed samples when compared to the original sample. Finally, energy estimations revealed that the proof-of-concept system operates at reduced energy requirements when compared to thermal drying systems thus presenting a promising prospect for an energy-efficient and economically sustainable alternative for CNF dewatering.

Acknowledgments The authors would like to acknowledge the support from Renewable Bioproducts Institute at Georgia Tech, Atlanta, USA. The authors would also like to thank the team from the Process Development Centre at University of Maine, Dr. Colleen Walker, Dr. Douglas Bousfield and Donna A. Johnson, for advising with the benchmarking experiments and providing samples.

Funding Renewable Bioproducts Institute, Georgia Tech, Atlanta, USA.

Data availablity All MATLAB code and data for this article are accessible here: https://github.com/bhamla-lab/Ultrasound_CNF_Dewatering2021

Declarations

Conflict of interest The authors declare no conflict of interest.

Consent for publication The authors consent for publication by the journal.

References

Al Zaitone B (2019) Drying kinetics of cellulose nanofibers suspensions. In: 21st international drying symposium. pp 11–14

Amini EN, Tajvidi M, Bousfield DW et al (2019) Dewatering behavior of a wood-cellulose nanofibril particulate system. Sci Rep 9(1):10. https://doi.org/10.1038/s41598-019-51177-x

Astorsdotter J (2017) Dewatering cellulose nanofibril suspensions through centrifugation

Baker CGJ, McKenzie KA (2005) Energy consumption of industrial spray dryers. Dry Technol 23:365–386. https://doi.org/10.1081/DRT-200047665

Beck S, Bouchard J, Berry R (2012) Dispersibility in water of dried nanocrystalline cellulose. Biomacromolecules 13:1486–1494

Beuguel Q, Tavares JR, Carreau PJ, Heuzey M (2018) Ultrasonication of spray-and freeze-dried cellulose nanocrystals in water. J Coll Interface Sci 516:23–33. https://doi.org/10.1016/j.jcis.2018.01.035

Boucher RMG (1959a) Ultrasonic boosts heatless drying.pdf. Chem Eng 66:151–154

Boucher RMG (1959b) Drying by airborne ultrasonics. Ultrason News 3:8–9

Clayton SA, Scholes ON, Hoadley AFA et al (2006) Dewatering of biomaterials by mechanical thermal expression. Dry Technol 24:819–834. https://doi.org/10.1080/07373930600733093

Čolić M, Tomić S, Bekić M (2020) Immunological aspects of nanocellulose. Immunol Lett 222:80–89. https://doi.org/10.1016/j.imlet.2020.04.004

Dimic-Misic K, Maloney T, Gane P (2018) Effect of fibril length, aspect ratio and surface charge on ultralow shear-induced structuring in micro and nanofibrillated cellulose aqueous suspensions. Cellulose 25:117–136. https://doi.org/10.1007/s10570-017-1584-3

Dimic-Misic K, Maloney T, Liu G, Gane P (2017) Micro nanofibrillated cellulose (MNFC) gel dewatering induced at ultralow-shear in presence of added colloidally-unstable particles. Cellulose 24:1463–1481. https://doi.org/10.1007/s10570-016-1181-x

Dimic-Misic K, Puisto A, Paltakari J et al (2013) The influence of shear on the dewatering of high consistency nanofibrillated cellulose furnishes. Cellulose 20:1853–1864. https://doi.org/10.1007/s10570-013-9964-9

Engineering Toolbox (2010) Water-heat of vaporization. https://www.engineeringtoolbox.com/water-properties-d_1573.html. Accessed 4 Jun 2021

Foster EJ, Moon RJ, Heux L et al (2018) Current characterization methods for cellulose nanomaterials. Chem Soc Rev 47:2609–2679. https://doi.org/10.1039/c6cs00895j

Gallego-Juárez JA, Riera E, de la Fuente BS et al (2007) Application of high-power ultrasound for dehydration of vegetables: processes and devices. Dry Technol 25:1893–1901. https://doi.org/10.1080/07373930701677371

Gallego-Juárez JA, Rodriguez-Corral G, Moraleda JCG, Yang TS (1999) A new high-intensity ultrasonic technology for food dehydration. Dry Technol 17:597–608. https://doi.org/10.1080/07373939908917555

García-Pérez JV, Carcel JA, Mulet A, Riera E, Gallego-Juarez JA (2015) Ultrasonic drying for food preservation, Power ultrasonics. Elsevier, pp 875–910, https://doi.org/10.1016/B978-1-78242-028-6.00029-6

Geng L, Mittal N, Zhan C et al (2018) Understanding the mechanistic behavior of highly charged cellulose nanofibers in aqueous systems. Macromolecules 51:1498–1506. https://doi.org/10.1021/acs.macromol.7b02642

Greguss P (1963) The mechanism and possible applications of drying by ultrasonic irradiation. Ultrasonics 1:83–86. https://doi.org/10.1016/0041-624X(63)90059-3

Han J, Zhou C, Wu Y et al (2013) Self-assembling behavior of cellulose nanoparticles during freeze-drying: effect of suspension concentration, particle size, crystal structure, and surface charge. Biomacromolecules 14:1529–1540. https://doi.org/10.1021/bm4001734

Hanif Z, Jeon H, Tran TH et al (2018) Butanol-mediated oven-drying of nanocellulose with enhanced dehydration rate and aqueous re-dispersion. J Polym Res 25:191

Iwamoto S, Nakagaito AN, Yano H, Nogi M (2005) Optically transparent composites reinforced with plant fiber-based nanofibers. Appl Phys A 1112:1109–1112. https://doi.org/10.1007/s00339-005-3316-z

Kelly PV, Gardner DJ, WMGramlich (2021) Optimizing lignocellulosic nanofibril dimensions and morphology by mechanical refining for enhanced adhesion. Carbohyd Polym 273:11856. https://doi.org/10.1016/j.carbpol.2021.118566

Miller T, Kramer C, Fisher A (2015) Bandwidth study on energy use and potential energy saving opportunities in U.S. pulp and paper manufacturing. US Dep Energy

Missoum K, Bras J, Belgacem MN (2012) Water redispersible dried nanofibrillated cellulose by adding sodium chloride. Biomacromolecules 13:4118–4125

Moon RJ, Martini A, Nairn J et al (2011) Cellulose nanomaterials review: structure, properties and nanocomposites. Chem Soc Rev 40:3941. https://doi.org/10.1039/c0cs00108b

Musielak G, Mierzwa D, Kroehnke J (2016) Food drying enhancement by ultrasound–a review. Trends Food Sci Technol 56:126–141. https://doi.org/10.1016/j.tifs.2016.08.003

Nigmatullin R, Johns MA, Muñoz-García JC et al (2020) Hydrophobization of cellulose nanocrystals for aqueous colloidal suspensions and gels. Biomacromolecules 21:1812–1823. https://doi.org/10.1021/acs.biomac.9b01721

Park C-W, Han S-Y, Namgung H-W et al (2017) Effect of spray-drying condition and surfactant addition on morphological characteristics of spray-dried nanocellulose. J Environ Sci 33:33–38. https://doi.org/10.7747/jfes.2017.33.1.33

Patel DK, Dutta SD, Lim KT (2019) Nanocellulose-based polymer hybrids and their emerging applications in biomedical engineering and water purification. RSC Adv 9:19143–19162. https://doi.org/10.1039/c9ra03261d

Peng Y, Gardner DJ (2013) Influence of drying method on the material properties of nanocellulose I: thermostability and crystallinity. Cellulose 20:2379–2392

Peng Y, Gardner DJ, Han Y (2012a) Drying cellulose nanofibrils: in search of a suitable method. Cellulose 19:91–102. https://doi.org/10.1007/s10570-011-9630-z

Peng Y, Gardner DJ, Han Y (2012b) Drying cellulose nanofibrils : morphology characterization. In: 55th international convention of society of wood science and technology. pp 1–9

Peng Y, Gardner DJ, Han Y et al (2013) Influence of drying method on the surface energy of cellulose nanofibrils determined by inverse gas chromatography. J Colloid Interface Sci 405:85–95. https://doi.org/10.1016/j.jcis.2013.05.033

Peng C, Momen AM, Moghaddam S (2017a) An energy-efficient method for direct-contact ultrasonic cloth drying. Energy 138:133–138. https://doi.org/10.1016/j.energy.2017.07.025

Peng C, Ravi S, Patel VK et al (2017b) Physics of direct-contact ultrasonic cloth drying process *. Energy 125:498–508. https://doi.org/10.1016/j.energy.2017.02.138

Penttila PA, Ra P, Maunu SL et al (2012) The effect of drying method on the properties and nanoscale structure of cellulose whiskers. Cellulose 901:912. https://doi.org/10.1007/s10570-012-9695-3

Quiévy N, Jacquet N, Sclavons M et al (2010) Influence of homogenization and drying on the thermal stability of microfibrillated cellulose. Polym Degrad Stab 95:306–314

Rantanen J, Maloney TC (2015) Consolidation and dewatering of a microfibrillated cellulose fiber composite paper in wet pressing. Eur Polym J 68:585–591. https://doi.org/10.1016/j.eurpolymj.2015.03.045

Rebouillat S, Pla F (2013) State of the art manufacturing and engineering of nanocellulose: a review of available data and industrial applications. J Biomater Nanobiotechnol 04:165–188. https://doi.org/10.4236/jbnb.2013.42022

Sabarez H, Swiergon P, Knoerzer K (2019) Drying process and apparatus

Sehaqui H, Liu A, Zhou Q, Berglund LA (2010) Fast preparation procedure for large, flat cellulose and cellulose/inorganic nanopaper structures. Biomacromolecules 2195:2198

Sethi J, Oksman K, Illikainen M, Sirviö JA (2018) Sonication-assisted surface modification method to expedite the water removal from cellulose nanofibers for use in nanopapers and paper making. Carbohydr Polym 197:92–99. https://doi.org/10.1016/j.carbpol.2018.05.072

Sim K, Lee J, Lee H, Youn HJ (2015) Flocculation behavior of cellulose nanofibrils under different salt conditions and its impact on network strength and dewatering ability. Cellulose 22:3689–3700. https://doi.org/10.1007/s10570-015-0784-y

Sinquefield S, Ciesielski PN, Li K et al (2020) Nanocellulose dewatering and drying: current state and future perspectives. ACS Sustain Chem Eng 8:9601–9615. https://doi.org/10.1021/acssuschemeng.0c01797

UMaine The Process development Center (2021) https://umaine.edu/pdc/nanocellulose/. Accessed 7 Jul 2021

Wetterling J, Jonsson S, Mattsson T, Theliander H (2017) The influence of ionic strength on the electroassisted filtration of microcrystalline cellulose. Ind Eng Chem Res 56:12789–12798. https://doi.org/10.1021/acs.iecr.7b03575

Wetterling J, Sahlin K, Mattsson T et al (2018) Electroosmotic dewatering of cellulose nanocrystals. Cellulose 25:2321–2329. https://doi.org/10.1007/s10570-018-1733-3

Zhai L, Kim HC, Kim JW, Kim J (2020) Simple centrifugal fractionation to reduce the size distribution of cellulose nanofibers. Sci Rep 10(1):1–8. https://doi.org/10.1038/s41598-020-68642-7

Zimmermann MVG, Borsoi C, Lavoratti A et al (2016) Drying techniques applied to cellulose nanofibers. J Reinf Plast Compos 35:682–697. https://doi.org/10.1177/0731684415626286